

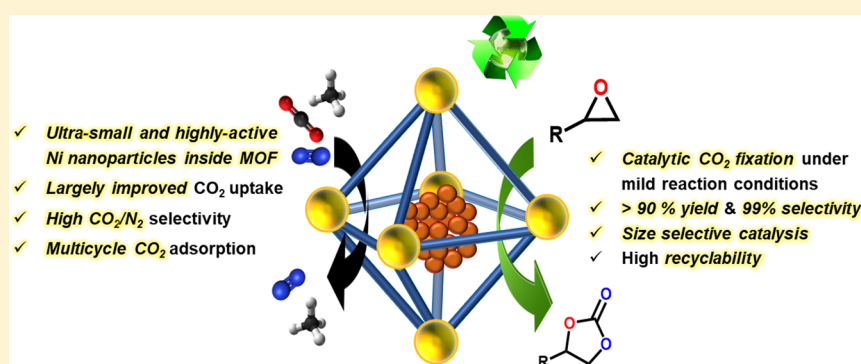
Highly Active Ultrasmall Ni Nanoparticle Embedded Inside a Robust Metal–Organic Framework: Remarkably Improved Adsorption, Selectivity, and Solvent-Free Efficient Fixation of CO₂

Manpreet Singh,^{‡,†} Pratik Solanki,[†] Parth Patel,[†] Aniruddha Mondal,^{‡,†} and Subhadip Neogi^{*,‡,†}

[†]Inorganic Materials & Catalysis Division, CSIR-Central Salt and Marine Chemicals Research Institute (CSMCRI), Bhavnagar, Gujarat 364002, India

[‡]Academy of Scientific and Innovative Research (AcSIR), CSIR-CSMCRI, G. B. Marg, Bhavnagar, Gujarat 364 002, India

S Supporting Information



ABSTRACT: We report integrating additional functionality in an amine decorated, robust metal–organic framework (MOF) by encapsulating Ni nanoparticles (NPs). In-depth characterization of the postmodified structure confirms well-dispersed and ultrasmall NPs inside the framework pores. Although, the surface area is more reduced than pristine MOF, the CO₂ uptake capacity is remarkably increased by 35% with a large 10 kJ/mol rise in adsorption enthalpy that validates favorable interactions between CO₂ and NPs. In particular, CO₂ adsorption selectivity over N₂ and CH₄ displays significant improvement (CO₂/N₂ = 145.7, CO₂/CH₄ = 12.65), while multicycle CO₂ uptake demonstrates outstanding sorption recurrence. Impressively, the embedded NPs act as highly active functional sites toward solvent-free CO₂ cycloaddition with epoxides in 98% yield and 99% selectivity under relatively mild conditions. The catalyst shows high recyclability without leaching of any metal-ion/NPs and greater pre-eminent activity than the unmodified analogue or contemporary reports. Of note is that outstanding conversion and selectivity are maintained for a wide range of aliphatic and aromatic epoxides, while larger substrates exhibit insignificant conversion, demonstrating admirable size selectivity. Based on the literature reports and experimental outcome, a rationalized mechanism is proposed for the reaction. This study exclusively demonstrates how strategic encapsulation of Ni NPs influences the inherent electronic properties in a MOF for highly selective CO₂ adsorption and represents a step forward to sustainable CO₂ valorization in terms of abundant active sites, sufficient stability, and consistent usability.

INTRODUCTION

The continued use of fossil fuels is anticipated for many years to come, owing to the slow rate of transition toward renewable and clean energy sources.¹ Consequently, the concentration of the central greenhouse pollutant carbon dioxide (CO₂) has already surpassed the level of 400 ppm and continues to accumulate more in the atmosphere at an alarming rate. Henceforth, CO₂ capture, sequestration (CCS) and its chemical transformation are the areas of intense current interest.^{2–4} Although, postcombustion CO₂ capture from flue gas is considered as the easiest capture process, this feat is tricky owing to the minimal differences in molecules present in the main components of this gas (CO₂ and N₂). As such, their effective separation requires tailor-made adsorbents with molecule-specific chemical interactions on their internal

surface. Alternatively, the nontoxicity and easy obtainability of anthropogenic CO₂ opens up its potential as a valid C1 source in the manufacture of several value-added compounds.^{5–7} In particular, the valorization of CO₂ with epoxides to yield cyclic carbonate is a 100% atom economic and attractive strategy^{8,9} due to the extensive application of the product in pharmaceuticals,¹⁰ as precursors in fine chemicals,¹¹ electrolytic elements of batteries,¹² polar aprotic solvents,¹³ and in polymer synthesis.¹⁴ However, the major flaw in this reaction is the chemical inertness of CO₂ that demands backing of a catalyst. In this connection, homogeneous catalysts are most effective, yet they seriously suffer from separation difficulties.¹⁵

Received: March 22, 2019

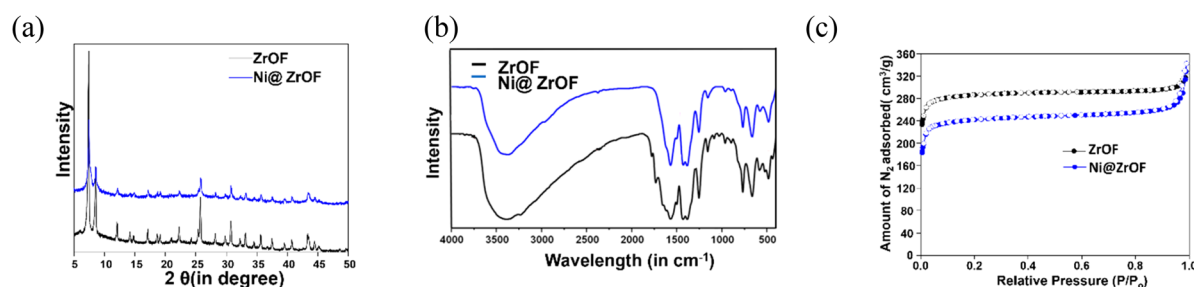


Figure 1. (a) PXRD pattern of ZrOF (as synthesized) and Ni@ZrOF, (b) IR spectra of ZrOF and Ni@ZrOF, and (c) N₂ adsorption isotherms of ZrOF and Ni@ZrOF.

Alternatively, complications from heterogeneous catalysts mostly stem from their inadequate activities, requirement for solvent assistance, and harsh reaction conditions. Thus, rational design of an acid–base multifunctional catalyst with good recyclability is imperative that can work even under mild conditions.^{16,17} Metal–organic frameworks (MOFs) are outstandingly porous, crystalline materials with a tunable pore surface and are highly promising candidates for a multitude of potential applications.^{18,19} In fact, selective CO₂ adsorption and the catalytic cycloaddition between CO₂ and epoxides in MOFs is an expanding area of interest.^{20–23} However, most of the MOF-based CO₂ adsorption systems lack enough stability, show moderate to low adsorbate–adsorbent interaction, and fail to produce high CO₂ adsorption selectivity. On the other hand, the catalytic performance is relatively poor for epoxide-based cycloaddition reactions in most of the MOFs, besides the fact that such reactions often require employment of solvents, very high temperature and pressure conditions, and extremely expensive ligands. Given both selective CO₂ adsorption and its efficient transformation principally requires presence of active functional sites, we focused on implementing additional functionality to synthesize *all in one* MOFs that can adsorb large amounts of CO₂ and facilitate the cycloaddition reaction under milder conditions.

Based on the above facts coupled with our quest to impart multifunctionality in a single MOF system,^{24–26} the present research strategy evolved by selecting Zr(IV) based frameworks that have gained particular interest owing to their high thermal as well as chemical stability, creation of open metal sites (OMS), and presence of unique large pores.^{27–29} We used the amine functionalized terephthalic acid linker to construct the well-known framework UiO-66-NH₂ (henceforth termed as ZrOF).³⁰ With a view to impart additional functionality and manipulate electronic property of the system, we aimed to incorporate metal nanoparticles (NPs) inside the pore via postsynthetic modification (PSM). It should be mentioned that encapsulation of metal NPs through PSM inside the large pores of MOFs is an emergent area of research, where the modified systems exhibit promising applications as diverse as gas storage,³¹ organic transformation,³² photocatalysis,³³ sensing,³⁴ and so on.³⁵ In this *modus operandi*, however, aggregation of NPs on the crystal surface is often inevitable, while repeated loading of precursors may also disrupt the targeted frameworks even under solvent-free vapor deposition conditions. On the other hand, most of such reports involve costly metal precursors^{36,37} that prompted us to use low-cost transition metal ions. Indeed, there is continued urge for the successful loading of cheap metal NPs inside the pores of MOFs.^{38,39} This observation led us to functionalize ZrOF with Ni NPs. Essentially, Ni is a relatively inexpensive and versatile catalyst

that should allow the Ni NP embedded MOF to show unique and/or improved properties, as illustrated for the Ni-supported carbon or silica materials.⁴⁰ Nevertheless, to our knowledge, only a handful of examples exist involving the preparation of Ni NPs inside the cavity of a MOF,^{41–43} while no report is available for any Zr(IV)-based frameworks. The NP embedded framework (Ni@ZrOF) was characterized by a battery of experimental evidence including Fourier transform-infrared (FT-IR), powder X-ray diffraction (PXRD), transmission electron microscopy (TEM), scanning electron microscopy-energy dispersive X-ray (SEM-EDAX), X-ray photoelectron spectroscopy (XPS), Raman spectroscopy, and inductively coupled plasma-atomic emission spectroscopy (ICP-AES), which corresponds to the successful encapsulation of well-dispersed and ultrasmall Ni NPs inside the pores. Although, inclusion of Ni NPs decreases the Brunauer–Emmett–Teller (BET) surface area compared to the pristine ZrOF, the CO₂ uptake capacity, isosteric heats of CO₂ adsorption, and CO₂ adsorption selectivity over N₂ and CH₄ show remarkable enhancement. These findings clearly validate improved interactions between polarizable CO₂ molecules and Ni NPs in a postmodified framework. Furthermore, the Ni@ZrOF system together with cocatalyst tetrabutyl ammonium bromide (TBAB) acts as an efficient, recyclable catalyst toward solvent-free cycloaddition of CO₂ and epoxides under relatively mild conditions. Impressively, the catalyst provided a much superior yield of cyclic carbonate compared to the nonmodified framework as well as most of the reported MOFs. Substrate variation studies demonstrated excellent size selectivity of the catalyst, where outstanding conversion and selectivity are maintained for a wide range of aliphatic and aromatic epoxides, while larger substrates showed negligible product yields.

RESULTS AND DISCUSSION

Synthesis and Characterization of Ni@ZrOF. The established framework UiO-66-NH₂ (hereafter termed as ZrOF) was solvothermally synthesized,⁴⁴ and formation of the desired structure was clearly verified upon cross-checking the experimental PXRD pattern (Figure 1a) to that of former reports.^{45,46} Infrared spectroscopy (Figure 1b) and thermogravimetric analyses (Figure S1) also confirm the formation of a phase pure ZrOF. The pore occluded solvent molecules in the as-synthesized framework were removed by solvent exchange followed by heat treatment at 120 °C under vacuum for 4 h. The permanent porosity was confirmed by the N₂ adsorption isotherms of guest-free ZrOF, which showed a BET surface area of 992 m²/g (Figure 1c).^{47,48} The value is lower than unfunctionalized UiO-66(Zr) because of the occupancy of pendent –NH₂ groups inside the MOF cavities. After complete characterization of phase pure ZrOF, synthesis of NP

Scheme 1. Synthesis of Ni@ZrOF Using the Solution Impregnation Method

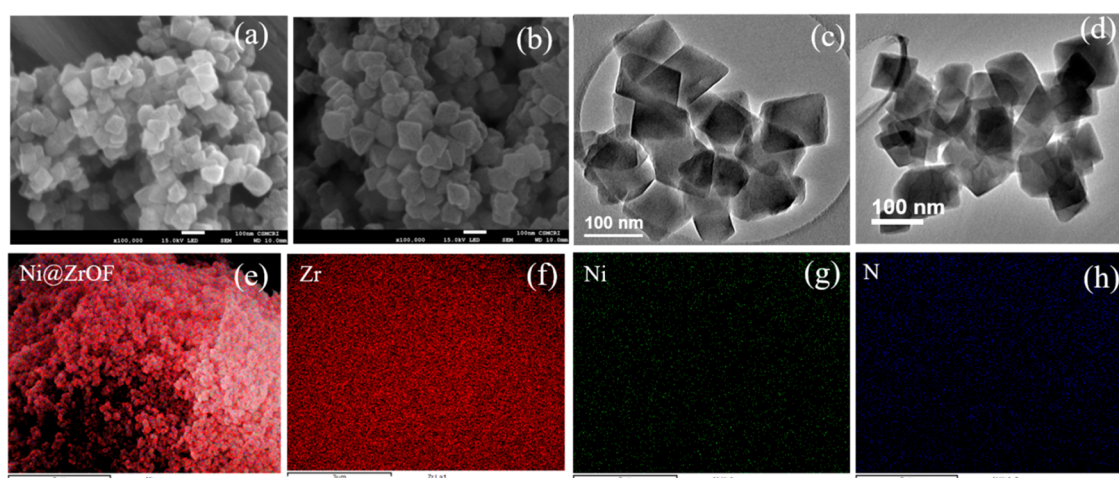
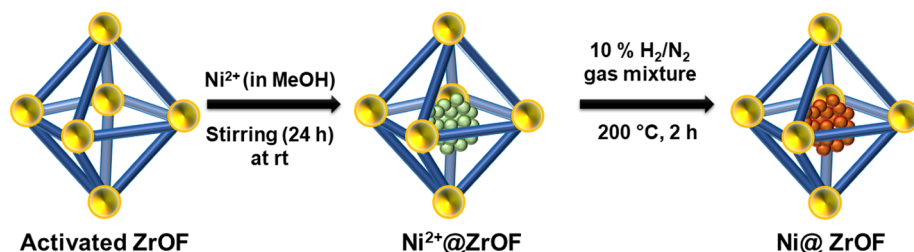


Figure 2. SEM images of the framework (a) ZrOF and (b) Ni@ZrOF and TEM images of the (c) ZrOF and (d) Ni@ZrOF. Elemental mapping of the Ni NP loaded framework (e–h) obtained from the SEM experiment.

embedded framework (Ni@ZrOF) was targeted by the solution impregnation method, followed by reduction of the material with a 10% H₂/N₂ gas mixture steam (Scheme 1). A comparison of the PXRD pattern of the postmodified framework to that of the parent material reveals exact correspondence of peak positions (Figure 1a), which imply that the addition of the Ni precursor and subsequent reduction treatment did not affect the stability of the framework. No characteristic diffraction peaks for metal nanoparticle (MNP) were observed throughout the 2θ range that can be related to the low metal contents in the postmodified material, as also realized in metal NP loaded MOFs.^{49,50}

Morphological investigation was performed for the corresponding ZrOF and metallic Ni loaded framework using field emission-scanning electron microscopy (FE-SEM), transmission electron microscopy (TEM), and high-resolution transmission electron microscopy (HRTEM). As shown in Figure 2a, the particle size from the SEM images was initially found in the range 100–130 nm. After incorporation of Ni nanoparticles into the ZrOF cavity, there is no obvious morphological change of the composite (Figure 2b). The low-resolution TEM images of the Ni@ZrOF clearly indicate the uniform size and shape (Figure 2d), with no apparent changes in particle sizes and morphology to that of the pristine framework. From HRTEM analysis, it was difficult to analyze the presence of ultrasmall metallic Ni nanoparticles due to the low Ni content (Figure S2). The presence of the corresponding element (Zr, C, N, O, and Ni) could be identified from SEM mapping on a selected area on the Ni@ZrOF composite (Figure 2), which divulged a homogeneous distribution of Ni, Zr, and N, suggesting that ultrasmall Ni nanoparticles were effectively encapsulated inside the modified framework (Figure

2e–h). The dispersion was uniform, and no sign of aggregation was observed. The SAED patterns (Figure S3) of ZrOF and ultrasmall MNP loaded material proved the polycrystalline nature in both the cases. Although, Raman spectroscopic studies were carried out to understand the ultrasmall nature of nickel nanoparticles, the presence of a highly fluorescent environment did not allow us to recognize the spectrum (Figure S4) unambiguously.⁵¹ The nickel content was determined by ICP-AES analysis, which displayed a loading of 1.12% of metal ions in the digested Ni@ZrOF framework. In addition, the quantity of Ni²⁺ remaining in Ni²⁺@ZrOF was separately calculated. For this, the washed out portion during successive cleaning was collected every time and ICP analysis was carried out. The difference between the supplied and removed Ni²⁺ (during washing steps) corresponds to the nickel amount (1.15%) incorporated actually. Clearly, both the results are in complete harmony with each other.

Thermal stability and robustness of the material were studied by thermogravimetric analysis (TGA) under a N₂ atmosphere up to a temperature of 800 °C (Figure S1). Nearly 10% weight loss ensues around 400 °C for Ni@ZrOF, showing high stability of the postmodified framework. The sharp weight loss above 700 °C is attributed to thermal degradation of the material. Essentially, encapsulation of Ni nanoparticles in the pores of ZrOF did not affect the thermal stability of the framework. Besides, Fourier transform infrared spectrum (FTIR) of Ni@ZrOF was found almost identical to that of the pristine framework (Figure 1b), where characteristic asymmetric stretching frequencies of the C=O from coordinated carboxylate groups are clearly observed at 1571 and 1497 cm⁻¹, while symmetric stretching frequencies are present at 1424 and 1381 cm⁻¹. The C–N vibrations, related to

amino groups, are also visible at 1335 and 1256 cm^{-1} . In addition, two peaks around 3470 and 3360 cm^{-1} are attributed to the asymmetric and symmetric stretching absorptions of the primary amine group that can be clearly discerned over the as made and postmodified samples. These two peaks are down shifted in comparison with pure $\text{NH}_2\text{-H}_2\text{BDC}$ (3500 and 3400 cm^{-1} , respectively), indicating that the amino groups are retained.⁵²

To further explore the chemical composition and oxidation states in ZrOF and Ni@ZrOF, XPS was adopted. The XPS survey spectrum (Figure 3) confirms the existence of Zr, Ni, O,

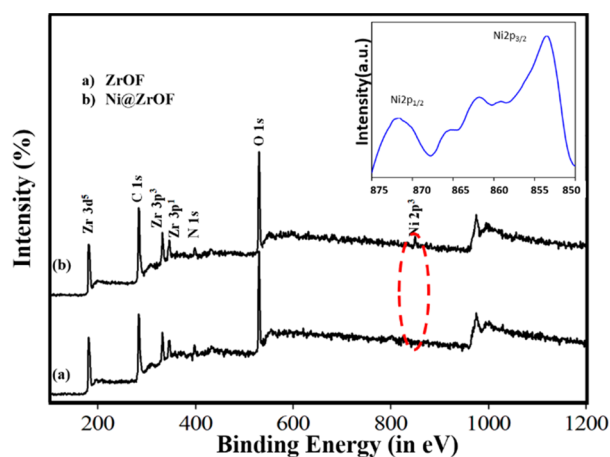


Figure 3. XPS survey spectra of (a) ZrOF and (b) Ni@ZrOF. Inset shows the Ni_{2p} spectrum.

N, and C in the modified sample. The intensity of the Ni peak was low due to the small nickel content in Ni@ZrOF (*vide supra*). To further clarify the oxidation state of the embedded Ni, the Ni_{2p} spectrum was closely crosschecked (Figure 3), which revealed that two peaks centered around 853 ($2p_{3/2}$) and 871 ($2p_{1/2}$) eV correspond to the Ni NPs. Besides, the N 1s peak in Ni@ZrOF is a bit shifted compared to ZrOF (Figure S5) that is most likely due to the noncovalent interaction between Ni NPs and the Lewis basic -NH_2 functionalities in the pore structure. This observation additionally supports the incorporation of small Ni nanoparticles inside the cavity only.⁵³

The N_2 adsorption–desorption isotherms at 77 K are presented in Figure 1c. While the BET surface area of ZrOF is found to be 992 m^2/g (*vide supra*), the value for Ni@ZrOF approximates to 898 m^2/g . Although, both the materials exhibit typical type I adsorption isotherms, indicating a microporous nature, the sharp reduction in the surface area can be attributed to the occupancy of the MNPs. Also, the total pore volume of ZrOF and Ni@ZrOF are found to be 0.46 and 0.40 cm^3/g , respectively (Table S1). Such a reduction in (a) N_2 adsorption amounts, (b) BET surface area, as well as (c) pore volume of Ni@ZrOF, as compared to the pristine ZrOF, collectively validates that the Ni nanoparticles are occupied inside the pores of framework. It should be noted that modified BET surface area is still adequate to supply more surface active sites for enhanced adsorption or catalysis.

CO_2 Adsorption and Selectivity in Ni@ZrOF. Given the importance to develop new protocols to reduce massive CO_2 emission, together with the fact that CO_2 adsorption capacity of a framework can be developed by added functionality,^{54,55} we aimed at probing Ni@ZrOF for CO_2 adsorption measurements

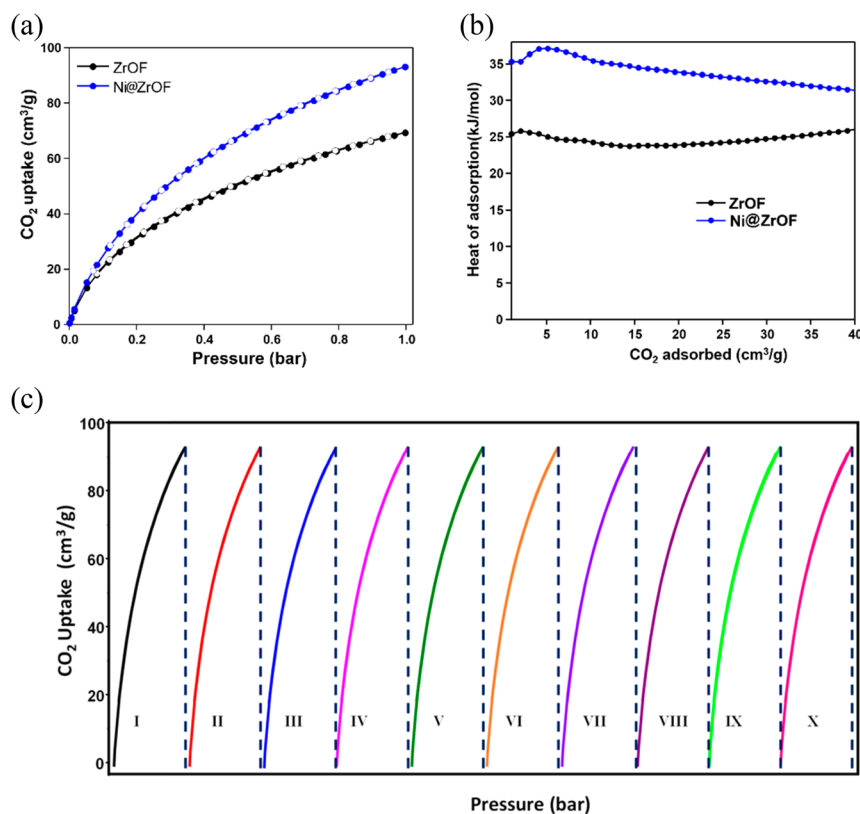


Figure 4. CO_2 adsorption isotherms for (a) ZrOF and Ni@ZrOF at 273 K. (b) Q_{st} curve of CO_2 adsorption of ZrOF and Ni@ZrOF. (c) Sorption recurrence during 10 cycles of CO_2 uptake at 273 K for Ni@ZrOF.

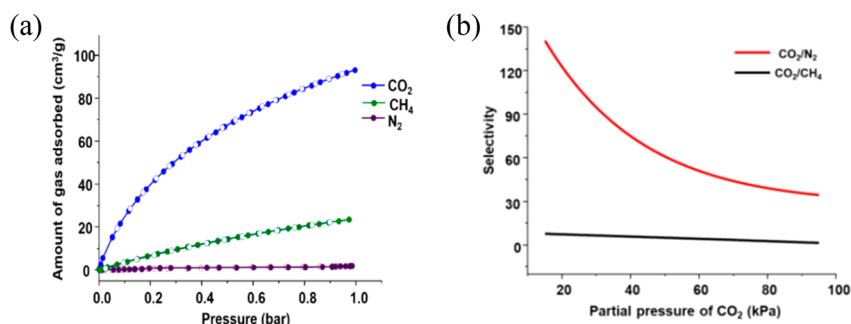


Figure 5. Gas adsorption isotherms for (a) Ni@ZrOF at 273 K and (b) IAST selectivity curves for CO₂/N₂ (red) and CO₂/CH₄ (black) for Ni@ZrOF at 273 K.

at different temperatures. At the onset, a thorough literature survey indicated no available reports of CO₂ sorption studies in metal NP loaded ZrOF and/or its isoreticular analogues (UiO-67, UiO-68). In contrast to low N₂ adsorption of postmodified framework, CO₂ adsorption capacity of the same material showed a remarkable uptake of 93.3 cm³/g (4.16 mmol/g) at 273 K, which is approximately 35% superior to that of parent ZrOF (Figure 4a). Notably, adsorption and desorption curves indicate no hysteresis. Further, the regenerative feature and nondestructive nature of Ni@ZrOF toward CO₂ adsorption was examined. To our delight, 10 cycles of CO₂ uptake at 273 K exhibit almost identical capacities with minor loss (Figure 4c), validating remarkable sorption recurrence. Moreover, the PXRD profile of Ni@ZrOF at the end of the adsorption–desorption cycles shows complete agreement to that of its original structural characteristics (Figure S7). No apparent saturation was observed within the studied pressure range (1.0 bar), signifying that more gas can be adsorbed by a further increase in pressure. The uptake value at 295 K (Figure S6) approximates to 55.6 cm³/g (2.48 mmol/g), which is ~11% more than that of pristine ZrOF under similar measurement conditions.⁵⁶ Interestingly, it appears that the N₂ adsorption based BET surface area of the metal-loaded MOF is not directly connected to its CO₂ adsorption capacity. In fact, the quantity of CO₂ adsorbed in Ni@ZrOF (18.3 wt %) is much higher than reported MOFs possessing similar surface areas and even comparable with some highly porous MOFs (based on surface areas). For instance, SNU-6, Y-FTZBP, rht-MOF-1, TTF-4, BIF-9-Li, and JLU-Liu31 (Table S4, entries 1–6) showed CO₂ uptake values of 9.9, 15.6, 17.7, 13.3, 6.6, and 6.86 cm³/g, respectively, at 273 K. However, corresponding BET surface areas of all those MOFs are far superior than the present system. The sorption behaviors of Ni@ZrOF with respect to CH₄ and N₂ were also studied. The result at 273 K shows (Figure 5a) a maximum CH₄ uptake of 23.4 cm³/g (1.04 mmol/g, 1.67 wt %). However, the uptake of N₂ is negligible. These data validate that the Ni⁰ loaded pore structure is majorly available to CO₂ (kinetic diameter = 3.3 Å), which can facilitate selective CO₂ adsorption over other gases.

Clearly, the improved CO₂ adsorption capacity in the Ni nanoparticle incorporated structure can be attributed to the strong affinity between the polarizable CO₂ gas molecules (quadrupole moment, 13.4×10^{-40} C m²; polarizability, 26.3×10^{-25} cm³) and auxiliary adsorption sites on the surface of Ni NPs, besides free –NH₂ groups. To corroborate this statement, we further considered the isosteric heat of CO₂ adsorption (Q_{st}) from the Clausius–Clapeyron equation, using the isotherms at 273 and 295 K.⁵⁷ The calculated heat of

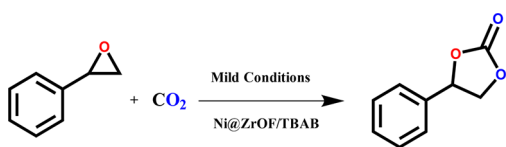
adsorption for Ni@ZrOF (36.20 kJ/mol) is found almost 10 kJ/mol higher than the framework (Figure 4b), devoid of MNPs (26.30 kJ/mol). Such improved value evidently highlights the significant role of encapsulated metal nanoparticles for providing additional interaction sites with adsorbate molecules. The Q_{st} value experiences a rise at low loading because of enhanced interaction between the polar CO₂ molecules and functional sites in the modified framework. The value decreases thereafter, owing to the filling of the maximum affinity sites and shows nearly maintenance of the plateau even at higher coverages. As displayed in Table S4, the obtained Q_{st} value is superior to many of the known MOFs. It is worth mentioning here that this reasonable enthalpy of adsorption offers not only a good affinity to CO₂ capture but also points to the easy adsorbent restoration, which is a vital and anticipated property for real-time applications.

To gain comprehensive understanding of the gas separation performance on Ni@ZrOF, the CO₂ gas selectivity (S) over N₂ and CH₄ were inspected by the ideal adsorbed solution theory (IAST) from single-component isotherms at 273 K (Figure 5b).^{58,59} To our knowledge, no NP encapsulated framework has so far been explored for CO₂ selectivity. The CO₂ selectivity over N₂ (CO₂/N₂ = 15:85 mole ratios) is calculated to be 145.7, which is more pre-eminent than the pristine MOF. Such a high value is rarely reported, and only a handful of frameworks have shown similar CO₂/N₂ selectivity (Table S3). The high CO₂/N₂ selectivity is primarily ascribed to the strong electrostatic interactions between diverse polar sites inside the pore and CO₂ molecules. We extended the IAST selectivity to CO₂/CH₄ as well, which is found to be 12.65 (Figure 5b). Although, CH₄ has a larger kinetic diameter (3.8 Å) than N₂ (3.64 Å), favorable adsorption of the former can be correlated to the larger polarizability of CH₄ (26×10^{-25} cm³) compared to N₂ (17.6×10^{-25} cm³). Even though, Ag-loaded porous materials have shown enhanced adsorption of Xe over Kr,⁶⁰ the present work represents a previously unreported illustration of how Ni⁰ can offer tremendous potential toward selective CO₂ adsorption.^{61,62}

Solvent Free Fixation of CO₂ to Cyclic-Carbonate.

Given that loading of NPs offers potential auxiliary binding sites to the CO₂ molecules, we wondered if this exclusive trifunctional system, encompassing open Brønsted-acid sites (Zr–OH/Zr–OH₂), Lewis basic –NH₂ groups, as well as highly active metal NPs, could promote chemical transformation of adsorbed CO₂ to cyclic carbonate. In a typical experiment, solvent-free CO₂ cycloaddition using model substrate styrene oxide (SO) was evaluated for the heterogeneous catalytic performance (Scheme 2).

Scheme 2. Cycloaddition Reaction of Styrene Oxide and CO₂



The initial screening reactions were performed under solvent-free conditions (Table 1), which displayed no styrene

Table 1. Screening of Various Catalysts for Cycloaddition of Styrene Oxide and CO₂^a

entry	catalyst	temperature (°C)	selectivity (%)	yield (%)
1	none	70	0	0
2	ZrCl ₄	70		
3	NH ₂ -BDC	70		
4	TBAB	70	98	25
5	ZrCl ₄ + NH ₂ -BDC + TBAB	70	98	30
6	ZrOF	70	99	41
7	Ni@ZrOF	70	99	45
8	ZrOF/TBAB	70	97	52
9	Ni ²⁺ @ZrOF/TBAB	70	98	62
10	Ni@ZrOF/TBAB	70	99	98
11	Ni@ZrOF/TBAI	70	99	83
12	Ni@ZrOF/TBAB	120	99	99

^aReaction conditions: SO, 30.6 mmol; catalyst, 0.35 mol %; cocatalyst, 0.11 mol %; CO₂ pressure, 1.0 MPa; 70 °C, 6 h.

carbonate (SC) transformation either under catalyst-free conditions (entry 1) or by using catalyst precursor materials (entries 2 and 3). On the other hand, ZrOF or Ni@ZrOF, as sole catalyst, produced only a moderate yield of SC (Table 1, entries 6 and 7). We also used tetrabutylammonium bromide (TBAB) as single catalyst that showed only a 25% yield of SC (Table 1, entry 4), while TBAB mixed with the precursor materials produced 30% yield (Table 1, entry 5). Surprisingly, when the reaction was performed in the presence of the Ni@ZrOF (0.35 mol % MOF) in association with TBAB (0.11 mol %), SC was obtained in 98% yield (Table 1, entry 10) under relatively mild reaction conditions (1.0 MPa CO₂ pressure, 70 °C temperature, 6 h). To understand whether the amine groups or the Ni NPs play the more significant role in cyclic carbonate synthesis, ZrOF/TBAB as well as Ni²⁺@ZrOF/TBAB systems were also investigated under similar conditions that produced 52 and 62% SC yields, respectively (Table 1, entries 8 and 9).

It should be noted that cycloaddition of CO₂ and SO has been previously investigated in ZrOF as well as in its nonaminated version (UiO-66), involving toxic chlorobenzene solvent that showed inferior results even under harsh reaction conditions (2.0 MPa, 100 °C).⁶³ The current results manifest the mutual effects of suitable acidity/basicity, microporosity, in combination with additional Ni NPs in the solventless catalysis under relatively milder conditions. Having recognized the combination of Ni@ZrOF/TBAB as a most effective system for chemical fixation of CO₂, we considered it worthwhile to match the efficiency of this system with the earlier reported MOFs. The collective results are furnished in Table S5, which shows that reactions over ZIFs and MOFs mostly require high-energy conditions (relatively high temperature and/or CO₂ pressure). Moreover, few catalysts like MOF-5 are prone to moisture,

while some MOF catalysts involve expensive ligands, which are unfavorable to practical usages. In contrast, the present system is based on inexpensive raw materials, requires milder reaction conditions, and exhibits better catalytic performance.

Effect of Reaction Parameters. Given temperature, pressure, time, and concentrations of reactants, catalyst, and cocatalyst display profound roles in SC formation, and all these parameters were thoroughly examined to determine the ideal conditions for maximum product yield. At the onset, the effect of catalyst amount in the cycloaddition reaction was investigated under semibatch operation conditions. As shown in Figure 6a, an increase in the yield of SC was evidenced when the amount of Ni@ZrOF was increased from 0 to 0.3 mol %. However, no promising development in the reaction was observed after reaching the maximal yield of 98% at 0.45 mol % of catalyst. This observation conceivably stems from the limitation in mass transfer between the catalyst active sites and reagent, caused by the lower dispersion of excess catalyst in the reaction mixture for achieving the reaction equilibrium.⁶⁴ As a part of the synergic Ni@ZrOF/TBAB system, the TBAB amount was also varied from 0.03 to 0.14 mol %, which shows 98% yield at 0.11 mol % (Figure 6c). In addition, the effect of anions in the tetraalkylammonium salt was studied by varying the halide ion. To our surprise, TBAB as cocatalyst rendered higher SC yield than its iodide analogue (TBAI). The result (Table 1, entry 11) indicates that despite its higher nucleophilicity, the diffusion of sterically demanding iodide ions into the pore is hampered in Ni@ZrOF.⁶⁵ In other words, the Ni@ZrOF/TBAI catalyst must have had superior activities than the Ni@ZrOF/TBAB system if the catalysis would occur on the surface of the framework. This fact evidently authenticates that the catalytic reaction occurs inside the optimized pores of the framework, and not on its external surface.

Apart from catalyst and cocatalyst, temperature is another significant factor that governs conversion of reactant to form thermodynamically and kinetically favored products. Besides, high reaction temperature needs to be avoided for this particular reaction to bypass the formation of unfavorable side products (diol).⁶⁶ As depicted in Figure 6b, the catalytic activity progressively increased from room temperature to 50 °C, and setting the temperature at 70 °C produced a maximum SC yield of 97%. A further increase in temperature had not much effect on the yield (Table 1, entry 12), which led us to execute all the reactions at 70 °C. Being the part of a synergic catalyst/cocatalyst/substrate system, the effects of varying pressure and time were also studied. As demonstrated in Figure 6d, yield of the product continuously increases by increasing pressure up to 1.0 MPa, and a further rise in pressure shows a trivial effect. This could be ascribed to the increasing solubility of CO₂ and consequent enrichment of CO₂ concentration in the reaction mixture up to the actual pressure that favors the equilibrium to shift to SC formation.⁶⁷ However, higher CO₂ pressure (1.2 MPa) decreases the concentration of SO in the liquid state. To check the yield of styrene carbonate as a function of time, study was conducted at different time intervals, which showed a maximum yield of 97.6% at 6 h. Further reaction continued up to 8 h and showed almost 99% yield (Figure 6e), with no catalyst poisoning effect. Therefore, the optimum conditions to obtain 97.6% yield of SC with 99% selectivity were identified as 1.0 MPa CO₂ pressure, 70 °C temperature, and 6 h duration.

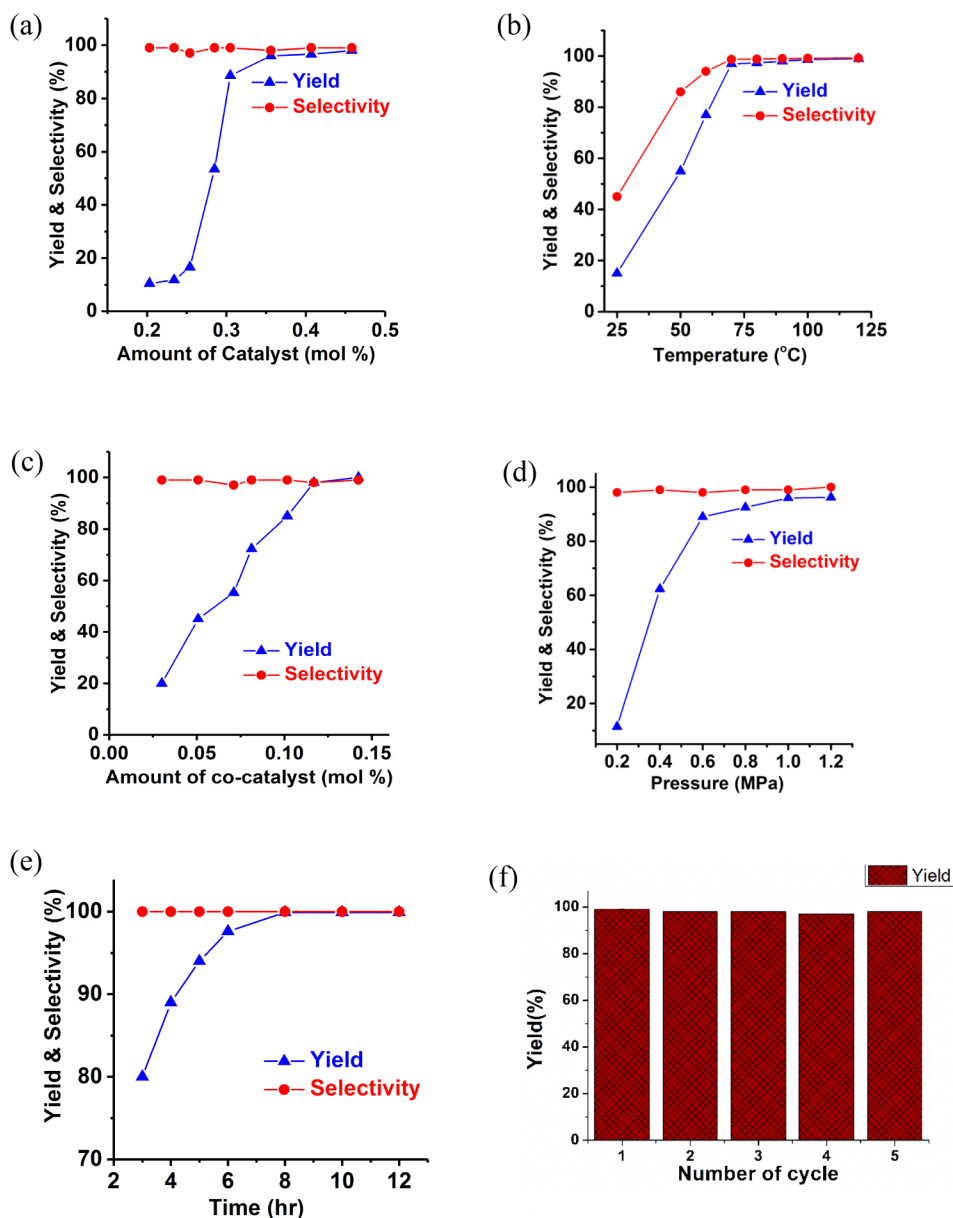


Figure 6. Effects of various reaction parameters on the yield and selectivity of SC (a) amount of catalyst, (b) temperature, (c) amount of cocatalyst, (d) CO₂ pressure, (e) time {reaction conditions: SO, 30.6 mmol (for parts a–e); catalyst, Ni@ZrOF 0.35 mol % (for parts b–e); TBAB co-catalyst, 0.11 mol % (for parts a, b, d, e); temperature, 70 °C (for parts a, c, d, e); pressure, 1.0 MPa (for parts a, b, c, e); duration, 6 h (for parts a–d)}, and (f) recyclability of the catalyst up to five cycles.

Catalyst Recyclability and Substrate Scope. To assess the recyclability and long-term stability of the catalyst, cycling experiments were undertaken under optimized conditions for the representative reaction (*vide supra*). The catalyst was separated from the reaction mixture via centrifugation (5000 rpm for 10 min) after each reaction run and reused in the next cycle. Impressively, gas chromatography (GC) analysis showed no significant loss in activity in up to five successive catalytic cycles (Figure 6f). The PXRD analysis on the reused Ni@ZrOF catalyst was performed after recycling studies, which showed that characteristic peaks remain unchanged (Figure S8). Additionally, FTIR analyses (Figure S9) and SEM imaging (Figure S10) provided further evidence that reused catalyst maintained the structural integrity and well-defined morphology. It is worth pointing out that Ni⁰ could come out from the catalyst pore during the reaction, which will eventually make

the entire catalyst less active for the subsequent cycles. To exclude such possibility, the reaction was continued with the filtrate in the absence of catalyst for additional 12 h that did not reveal any increase in the SC formation. At the culmination of the reaction, ICP-AES analysis was performed on the reaction mixture filtrate that showed no presence of the Ni and/or Zr. Alternatively, the recovered catalyst revealed that the amount of Ni and Zr in Ni@ZrOF remains almost unchanged. Nitrogen adsorption isotherms of fresh catalyst and used catalyst showed no significant change in N₂ adsorption (Figure S11), indicating integrity and porosity of the system are well maintained even after reaction. These collective results demonstrate that encapsulated nanoparticles never come out of the cavity during the reaction.

To ascertain the versatility of this catalytic system for CO₂ cycloaddition, we extended the reaction using different other

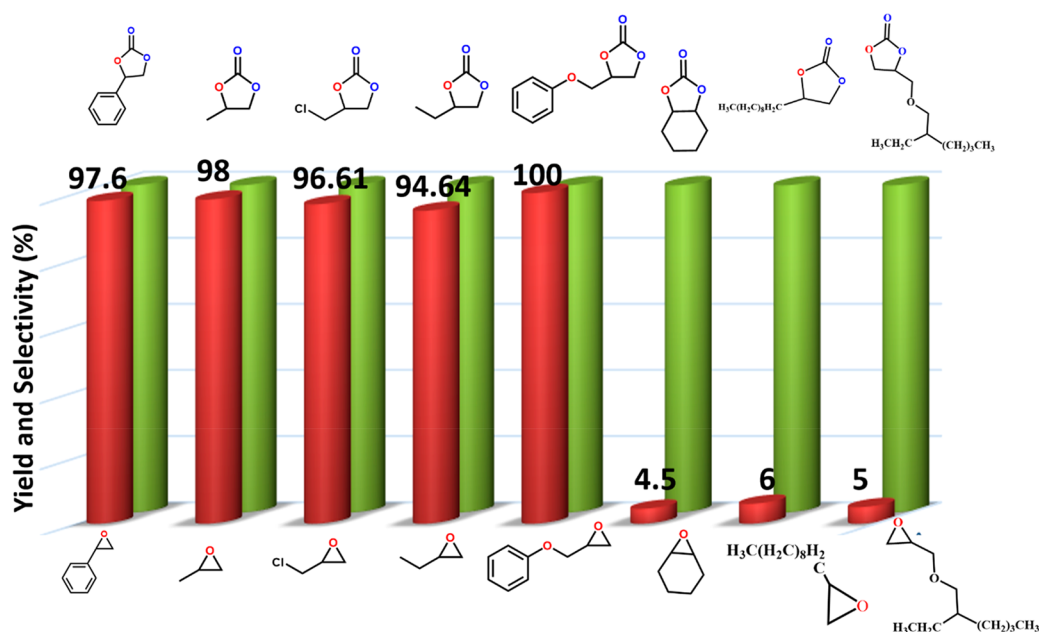


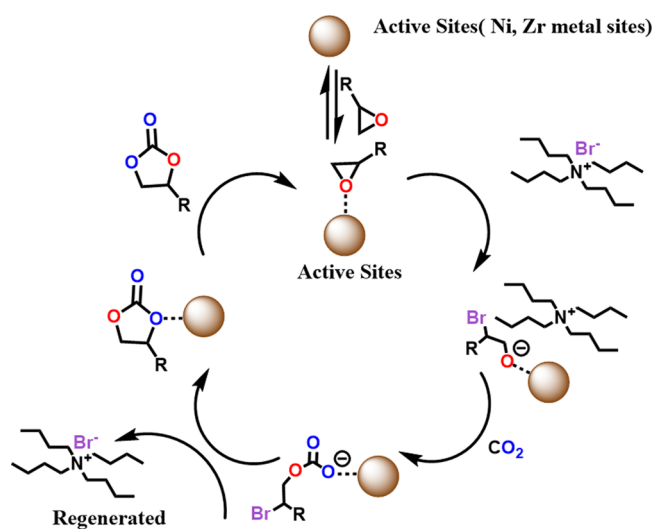
Figure 7. Substrate scope for Ni@ZrOF/Bu₄NBr catalytic system with yield (red) and selectivity (green). Optimized reaction conditions: epoxide, 30.6 mmol; Ni@ZrOF, 0.35 mol %; Bu₄NBr, 0.11 mol %; CO₂ pressure, 1.0 MPa; 70 °C, 6 h.

substrates under the optimized conditions. Since the experiments were conducted under solvent-free conditions, liquid substrates were selected (Figure 7). To the best of our catalytic system, high yields were preserved for a wide range of aliphatic as well as aromatic epoxides, producing more than 95% yield with very high selectivity in every case. These results are essentially better than those reported previously under comparable reaction conditions. However, cyclohexene oxide exhibits reasonably low yield of the analogous cyclic carbonate (4.5%) even though the reaction selectivity is found to be good. This inconsistency can be ascribed to the hindrance of anionic attack due to the steric crowding of the cyclohexene ring, as also recognized for other catalytic systems.^{68,69} On the other hand, larger substrates like 1,2-epoxydodecane, and 2-ethylhexyl glycidyl ether showed poor yields of just 6 and 5% (Figure 7), respectively. The sharp decrease in product yield suggests that larger substrates cannot diffuse inside the porous structure of Ni@ZrOF catalyst. Such size selective cycloaddition specifically points to the fact that reactions with other substrates occurred within the framework cavity rather than on the surface.

Mechanism for Catalytic Reaction. Given that the catalytic applications in MOF are a versatile and emerging branch of organic transformation with a heterogeneous manner, extending the synergistic insight among diverse active sites and their astute utilization will not only provide the comprehensive mechanistic pathways but also enrich the library of active catalysts with desirable properties. The high CO₂ adsorption potential together with the efficient catalytic performance of the Ni@ZrOF system are attributed to its unique hollow structure with Zr⁴⁺ acidic sites, incorporated Ni nanoparticle, and pendent -NH₂ groups that collectively manipulate the inherent electronic and surface properties of the host material. On the basis of the above results and previous other studies,^{70,71} we put forth a tentative mechanism for the cycloaddition reaction. Evidently, the catalytic performance of Ni@ZrOF is influenced by the synergistic effect of both Ni⁰ and Zr⁴⁺ metals, which promotes activation of the epoxide oxygen atom by distinct

active centers. This leads to minimization of the energy barrier of the reaction and increases the cyclic carbonate yield in comparison to what has so far been achieved by the sole Zr⁴⁺ center in ZrOF. This step triggers electrophilic attack toward the oxygen atom of the epoxide (Scheme 3), whereby ring

Scheme 3. Proposed Reaction Mechanism for the Cycloaddition of CO₂ and SO Using Synergic Ni@ZrOF/TBAB Catalyst



opening takes place by the attack of a Br⁻ ion from the cocatalyst TBAB on the less hindered carbon atom of the epoxide.^{72,73} Subsequently, the O⁻ of the epoxide ring attacks the carbon atom of the polarized CO₂ molecule, while the oxygen atom of the CO₂ molecule attacks the β-carbon of the ring opened epoxide after elimination of a bromide ion. It is worth mentioning that inside the autoclave reactor, we experienced a rapid decline in CO₂ pressure, which is indicative of an extremely supportive environment provided by the MOF

catalyst. Ring closure in the final step produces SC and consequently regenerates Ni@ZrOF, which is then transferred to the next cycle of cycloaddition by coordination with a new epoxide molecule.

■ EXPERIMENTAL SECTION

Synthesis of ZrOF. ZrOF was synthesized according to the previous report with slight modifications. $ZrCl_4$ (233 mg, 1 mmol) and NH_2-H_2BDC (181 mg, 1 mmol) were dissolved in 40 mL of DMF, and a small amount of water (0.150 mL, 8.3 mmol) was added to the solution. The mixture was sonicated for half an hour and transferred into a Teflon-lined stainless-steel autoclave. The autoclave was sealed and heated to 120 °C for 24 h. After cooling to room temperature, the yellow crystalline powder is collected by filtration and thoroughly washed with fresh DMF (3×10 mL times) and methanol (3×10 mL times) every 12 h. The yield of the yellow crystalline material obtained after air drying was 330 mg.

Synthesis of Ni@ZrOF. As described below, Ni@ZrOF metal composite was synthesized in two steps. The first step involves the incorporation of Ni^{2+} in ZrOF, and the second step is reduction of embedded metal ions to metal nanoparticles.

Synthesis of Ni^{2+} @ZrOF. Ni^{2+} @ZrOF has been prepared via the solution impregnation method. In a typical procedure, 1.0 g of activated ZrOF (obtained upon heating under vacuum at 120 °C for 5 h) was homogeneously dispersed in 100 mL of methanol by ultrasonication for 30 min. Then, $Ni(NO_3)_2 \cdot 6H_2O$ (100 mg) as the Ni^{2+} source (in 10 mL of methanol) was added dropwise to the ZrOF solution under vigorous stirring (to avoid agglomeration of metal particles) in a 250 mL round-bottom flask. Vigorous stirring was continued at 800 rpm for 24 h at room temperature. Afterward, Ni^{2+} @ZrOF was collected by centrifugation, washed three times with methanol to remove free/excess metal salt from the surface of ZrOF, and finally dried at 80 °C.

Conversion of Ni^{2+} @ZrOF to Ni@ZrOF. Calcination of the as synthesized Ni^{2+} @ZrOF was carried out in a tubular furnace under a steam of 10% H_2/N_2 gas mixture at 200 °C for 2 h at a ramp rate of 5 °C/min. During this process, Ni(II) was reduced and a dark yellow colored material was formed, which indicated the formation of MNPs inside ZrOF. The product was thoroughly characterized by means of several analytical techniques.

■ CONCLUSIONS

In summary, we report for the first time encapsulation of ultrasmall Ni nanoparticles (NPs) inside the pore of an amine grafted Zr(IV)-framework. The embedded Ni NPs act as additional functionality that in turn drastically improves the adsorption capacity of the major greenhouse gas CO_2 . The isosteric heat of CO_2 adsorption also experiences a 10 kJ/mol upsurge than the parent material, highlighting auxiliary interactions between CO_2 molecules and encapsulated NPs. Further, the postmodified system unveils excellent CO_2 selectivity over other gases and demonstrates remarkable sorption recurrences during multicycle CO_2 adsorption. The collective results render the NP loaded framework as a potential candidate for practical CO_2 sequestration applications. Most fascinatingly, the unique hollow structure, incorporated Ni NPs, and pendent basic functionality mutually manipulate the electronic environment of the pore, which allows outstanding heterogeneous catalytic performance toward solvent-free cycloaddition of CO_2 and epoxides under relatively mild conditions. It is imperative to stress that efficiency of catalyst is superior to many of the well-known MOFs and it can be recycled several times without metal leaching or significant loss in activity. The outstanding yield and selectivity of the catalyst are maintained for a wide range of aliphatic and aromatic epoxides, while larger substrates provide negligible conversion, corroborating admir-

able size selectivity. We put forth a tentative mechanism for the cycloaddition reaction on the basis of literature reports and experimental outcome. In a nutshell, the present system represents a valuable family member of MOFs to future heterogeneous catalysis in terms of abundant active sites, high stability, and sufficient reusability and supplements the suitability in extending its scope from academia and research to industrial perspectives.

■ ASSOCIATED CONTENT

Supporting Information

The Supporting Information is available free of charge on the ACS Publications website at DOI: [10.1021/acs.inorgchem.9b00833](https://doi.org/10.1021/acs.inorgchem.9b00833).

Materials and physical measurements; experimental section; TGA curves; HRTEM and SEM images; SAED patterns; Raman and XPS spectra; BET results; adsorption curves; PXRD, FTIR, and NMR spectra; pore volume and surface areas on the basis of N_2 and CO_2 adsorption isotherms; fitted parameters for adsorption isotherms at 273 K, CO_2/N_2 , and CO_2/CH_4 adsorption selectivity; comparison table for CO_2 adsorption capacity, isosteric heat of CO_2 adsorption, and Q_{st} for various MOFs; and comparison of catalytic activities of Ni@ZrOF catalyst with previously reported MOFs (PDF)

■ AUTHOR INFORMATION

Corresponding Author

*E-mail: sneogi@csmcri.res.in.

ORCID

Manpreet Singh: 0000-0002-0335-6147

Pratik Solanki: 0000-0002-1440-7931

Parth Patel: 0000-0001-9742-2784

Aniruddha Mondal: 0000-0002-5742-4459

Subhadip Neogi: 0000-0002-3838-4180

Notes

The authors declare no competing financial interest.

■ ACKNOWLEDGMENTS

S.N. acknowledges DST-SERB (Grant No. ECR/2016/000156) and CSIR (Grant No. MLP-0028). M.S. acknowledges UGC, Delhi, for providing a junior research fellowship. A.M. and P.P. acknowledge CSIR for senior research fellowships. P.S. acknowledges Manipal University for the M.Sc. internship. The analytical support from ADCIF is greatly acknowledged. This Article is CSMCRI Communication No. 003/2019.

■ REFERENCES

- (1) Liu, J.; Thallapally, P. K.; McGrail, B. P.; Brown, D. R.; Liu, J. Progress in adsorption-based CO_2 capture by metal-organic frameworks. *Chem. Soc. Rev.* **2012**, *41*, 2308–22.
- (2) D'Alessandro, D. M.; Smit, B.; Long, J. R. Carbon dioxide capture: prospects for new materials. *Angew. Chem., Int. Ed.* **2010**, *49*, 6058–82.
- (3) Solomon, S.; Plattner, G. K.; Knutti, R.; Friedlingstein, P. Irreversible climate change due to carbon dioxide emissions. *Proc. Natl. Acad. Sci. U. S. A.* **2009**, *106*, 1704–9.
- (4) Wang, H.-H.; Shi, W.-J.; Hou, L.; Li, G.-P.; Zhu, Z.; Wang, Y.-Y. A Cationic MOF with High Uptake and Selectivity for CO_2 due to Multiple CO_2 -Philic Sites. *Chem. - Eur. J.* **2015**, *21*, 16525–16531.

- (5) Lin, S.; Diercks, C. S.; Zhang, Y. B.; Kornienko, N.; Nichols, E. M.; Zhao, Y. B.; Paris, A. R.; Kim, D.; Yang, P.; Yaghi, O. M.; Chang, C. J. Covalent organic frameworks comprising cobalt porphyrins for catalytic CO₂ reduction in water. *Science* **2015**, *349*, 1208–1213.
- (6) Banerjee, A.; Dick, G. R.; Yoshino, T.; Kanan, M. W. Carbon dioxide utilization via carbonate-promoted C–H carboxylation. *Nature* **2016**, *531*, 215–219.
- (7) Wang, Y.; Zhang, J.; Qian, Q.; Asare Bediako, B. B.; Cui, M.; Yang, G.; Yan, J.; Han, B. Efficient synthesis of ethanol by methanol homologation using CO₂ at lower temperature. *Green Chem.* **2019**, *21*, 589–596.
- (8) Cokoja, M.; Bruckmeier, C.; Rieger, B.; Herrmann, W. A.; Kuhn, F. E. Transformation of carbon dioxide with homogeneous transition-metal catalysts: a molecular solution to a global challenge? *Angew. Chem., Int. Ed.* **2011**, *50*, 8510–37.
- (9) Li, Y.-Z.; Wang, H.-H.; Yang, H.-Y.; Hou, L.; Wang, Y.-Y.; Zhu, Z. An Uncommon Carboxyl-Decorated Metal–Organic Framework with Selective Gas Adsorption and Catalytic Conversion of CO₂. *Chem. - Eur. J.* **2018**, *24*, 865–871.
- (10) Pascual, A.; Tan, J. P.; Yuen, A.; Chan, J. M.; Coady, D. J.; Mecerreyes, D.; Hedrick, J. L.; Yang, Y. Y.; Sardon, H. Broad-spectrum antimicrobial polycarbonate hydrogels with fast degradability. *Biomacromolecules* **2015**, *16*, 1169–78.
- (11) Zhao, Y.; Yu, B.; Yang, Z.; Zhang, H.; Hao, L.; Gao, X.; Liu, Z. J. A. C. I. E. A Protic Ionic Liquid Catalyzes CO₂ Conversion at Atmospheric Pressure and Room Temperature: Synthesis of Quinazoline-2, 4 (1H, 3H)-diones. *Angew. Chem., Int. Ed.* **2014**, *53*, 5922–5925.
- (12) Petrowsky, M.; Ismail, M.; Glatzhofer, D. T.; Frech, R. Mass and charge transport in cyclic carbonates: implications for improved lithium ion battery electrolytes. *J. Phys. Chem. B* **2013**, *117*, 5963–70.
- (13) Parker, H. L.; Sherwood, J.; Hunt, A. J.; Clark, J. H. Cyclic Carbonates as Green Alternative Solvents for the Heck Reaction. *ACS Sustainable Chem. Eng.* **2014**, *2*, 1739–1742.
- (14) Gregory, G. L.; Kociok-Köhn, G.; Buchard, A. Polymers from sugars and CO₂: ring-opening polymerisation and copolymerisation of cyclic carbonates derived from 2-deoxy-d-ribose. *Polym. Chem.* **2017**, *8*, 2093–2104.
- (15) Kim, D.; Moon, Y.; Ji, D.; Kim, H.; Cho, D. Metal-Containing Ionic Liquids as Synergistic Catalysts for the Cycloaddition of CO₂: A Density Functional Theory and Response Surface Methodology Corroborated Study. *ACS Sustainable Chem. Eng.* **2016**, *4*, 4591–4600.
- (16) Wang, X.; Zhou, Y.; Guo, Z.; Chen, G.; Li, J.; Shi, Y.; Liu, Y.; Wang, J. Heterogeneous conversion of CO₂ into cyclic carbonates at ambient pressure catalyzed by ionothermal-derived meso-macroporous hierarchical poly(ionic liquid)s. *Chem. Sci.* **2015**, *6*, 6916–6924.
- (17) Han, Y.-H.; Zhou, Z.-Y.; Tian, C.-B.; Du, S.-W. A dual-walled cage MOF as an efficient heterogeneous catalyst for the conversion of CO₂ under mild and co-catalyst free conditions. *Green Chem.* **2016**, *18*, 4086–4091.
- (18) Kitagawa, S.; Kitaura, R.; Noro, S. Functional porous coordination polymers. *Angew. Chem., Int. Ed.* **2004**, *43*, 2334–75.
- (19) Silva, P.; Vilela, S. M. F.; Tomé, J. P. C.; Almeida Paz, F. A. Multifunctional metal–organic frameworks: from academia to industrial applications. *Chem. Soc. Rev.* **2015**, *44*, 6774–6803.
- (20) Kamphuis, A. J.; Picchioni, F.; Pescarmona, P. P. CO₂-fixation into cyclic and polymeric carbonates: principles and applications. *Green Chem.* **2019**, *21*, 406–448.
- (21) Babu, R.; Kathalikkattil, A. C.; Roshan, R.; Tharun, J.; Kim, D.-W.; Park, D.-W. Dual-porous metal organic framework for room temperature CO₂ fixation via cyclic carbonate synthesis. *Green Chem.* **2016**, *18*, 232–242.
- (22) Babu, R.; Roshan, R.; Kathalikkattil, A. C.; Kim, D. W.; Park, D. W. Rapid, Microwave-Assisted Synthesis of Cubic, Three-Dimensional, Highly Porous MOF-205 for Room Temperature CO₂ Fixation via Cyclic Carbonate Synthesis. *ACS Appl. Mater. Interfaces* **2016**, *8*, 33723–33731.
- (23) Li, X.-Y.; Ma, L.-N.; Liu, Y.; Hou, L.; Wang, Y.-Y.; Zhu, Z. Honeycomb Metal–Organic Framework with Lewis Acidic and Basic Bifunctional Sites: Selective Adsorption and CO₂ Catalytic Fixation. *ACS Appl. Mater. Interfaces* **2018**, *10*, 10965–10973.
- (24) Senthilkumar, S.; Goswami, R.; Obasi, N. L.; Neogi, S. Construction of Pillar-Layer Metal–Organic Frameworks for CO₂ Adsorption under Humid Climate: High Selectivity and Sensitive Detection of Picric Acid in Water. *ACS Sustainable Chem. Eng.* **2017**, *5*, 11307–11315.
- (25) Senthilkumar, S.; Goswami, R.; Smith, V. J.; Bajaj, H. C.; Neogi, S. Pore Wall-Functionalized Luminescent Cd(II) Framework for Selective CO₂ Adsorption, Highly Specific 2,4,6-Trinitrophenol Detection, and Colorimetric Sensing of Cu²⁺ Ions. *ACS Sustainable Chem. Eng.* **2018**, *6*, 10295–10306.
- (26) Senthilkumar, S.; Maru, M. S.; Somani, R. S.; Bajaj, H. C.; Neogi, S. Unprecedented NH₂-MIL-101(Al)/n-Bu₄NBr system as solvent-free heterogeneous catalyst for efficient synthesis of cyclic carbonates via CO₂ cycloaddition. *Dalton Trans.* **2018**, *47*, 418–428.
- (27) Furukawa, H.; Gándara, F.; Zhang, Y.-B.; Jiang, J.; Queen, W. L.; Hudson, M. R.; Yaghi, O. M. Water Adsorption in Porous Metal–Organic Frameworks and Related Materials. *J. Am. Chem. Soc.* **2014**, *136*, 4369–4381.
- (28) Bon, V.; Senkowska, I.; Weiss, M. S.; Kaskel, S. Tailoring of network dimensionality and porosity adjustment in Zr- and Hf-based MOFs. *CrystEngComm* **2013**, *15*, 9572–9577.
- (29) Feng, D.; Jiang, H.-L.; Chen, Y.-P.; Gu, Z.-Y.; Wei, Z.; Zhou, H.-C. Metal–Organic Frameworks Based on Previously Unknown Zr₈/Hf₈ Cubic Clusters. *Inorg. Chem.* **2013**, *52*, 12661–12667.
- (30) Cavka, J. H.; Jakobsen, S.; Olsbye, U.; Guillou, N.; Lamberti, C.; Bordiga, S.; Lillerud, K. P. A New Zirconium Inorganic Building Brick Forming Metal Organic Frameworks with Exceptional Stability. *J. Am. Chem. Soc.* **2008**, *130*, 13850–13851.
- (31) Ma, S.; Zhou, H.-C. Gas storage in porous metal–organic frameworks for clean energy applications. *Chem. Commun.* **2010**, *46*, 44–53.
- (32) An, B.; Zhang, J.; Cheng, K.; Ji, P.; Wang, C.; Lin, W. Confinement of Ultrasmall Cu/ZnO_x Nanoparticles in Metal–Organic Frameworks for Selective Methanol Synthesis from Catalytic Hydrogenation of CO₂. *J. Am. Chem. Soc.* **2017**, *139*, 3834–3840.
- (33) Li, Y.; Jiang, J.; Fang, Y.; Cao, Z.; Chen, D.; Li, N.; Xu, Q.; Lu, J. TiO₂ Nanoparticles Anchored onto the Metal–Organic Framework NH₂-MIL-88B(Fe) as an Adsorptive Photocatalyst with Enhanced Fenton-like Degradation of Organic Pollutants under Visible Light Irradiation. *ACS Sustainable Chem. Eng.* **2018**, *6*, 16186–16197.
- (34) Kreno, L. E.; Leong, K.; Farha, O. K.; Allendorf, M.; Van Duyne, R. P.; Hupp, J. T. Metal–Organic Framework Materials as Chemical Sensors. *Chem. Rev.* **2012**, *112*, 1105–1125.
- (35) Islamoglu, T.; Goswami, S.; Li, Z.; Howarth, A. J.; Farha, O. K.; Hupp, J. T. Postsynthetic Tuning of Metal–Organic Frameworks for Targeted Applications. *Acc. Chem. Res.* **2017**, *50*, 805–813.
- (36) Chen, L. N.; Zhan, W. W.; Fang, H. H.; Cao, Z. M.; Yuan, C. F.; Xie, Z. X.; Kuang, Q.; Zheng, L. S. Selective Catalytic Performances of Noble Metal Nanoparticle@MOF Composites: The Concomitant Effect of Aperture Size and Structural Flexibility of MOF Matrices. *Chem. - Eur. J.* **2017**, *23*, 11397–11403.
- (37) Ning, L.; Liao, S.; Cui, H.; Yu, L.; Tong, X. Selective Conversion of Renewable Furfural with Ethanol to Produce Furan-2-acrolein Mediated by Pt@MOF-5. *ACS Sustainable Chem. Eng.* **2018**, *6*, 135–142.
- (38) Isaka, Y.; Kondo, Y.; Kawase, Y.; Kuwahara, Y.; Mori, K.; Yamashita, H. Photocatalytic production of hydrogen peroxide through selective two-electron reduction of dioxygen utilizing amine-functionalized MIL-125 deposited with nickel oxide nanoparticles. *Chem. Commun.* **2018**, *54*, 9270–9273.
- (39) Bennedsen, N. R.; Kramer, S.; Mielby, J. J.; Kegnes, S. Cobalt–nickel alloy catalysts for hydrosilylation of ketones synthesized by utilizing metal–organic framework as template. *Catal. Sci. Technol.* **2018**, *8*, 2434–2440.

- (40) Yang, L. J.; Zhou, W. J.; Jia, J.; Xiong, T. L.; Zhou, K.; Feng, C. H.; Zhou, J.; Tang, Z. H.; Chen, S. W. Nickel nanoparticles partially embedded into carbon fiber cloth via metal-mediated pitting process as flexible and efficient electrodes for hydrogen evolution reactions. *Carbon* **2017**, *122*, 710–717.
- (41) Park, Y. K.; Choi, S. B.; Nam, H. J.; Jung, D.-Y.; Ahn, H. C.; Choi, K.; Furukawa, H.; Kim, J. Catalytic nickel nanoparticles embedded in a mesoporous metal–organic framework. *Chem. Commun.* **2010**, *46*, 3086–3088.
- (42) Zhen, W.; Ma, J.; Lu, G. Small-sized Ni(111) particles in metal–organic frameworks with low over-potential for visible photocatalytic hydrogen generation. *Appl. Catal., B* **2016**, *190*, 12–25.
- (43) Zhao, Z.-W.; Zhou, X.; Liu, Y.-N.; Shen, C.-C.; Yuan, C.-Z.; Jiang, Y.-F.; Zhao, S.-J.; Ma, L.-B.; Cheang, T.-Y.; Xu, A.-W. Ultrasmall Ni nanoparticles embedded in Zr-based MOFs provide high selectivity for CO₂ hydrogenation to methane at low temperatures. *Catal. Sci. Technol.* **2018**, *8*, 3160–3165.
- (44) Zhang, F. M.; Zheng, S.; Xiao, Q.; Zhong, Y. J.; Zhu, W. D.; Lin, A.; El-Shall, M. S. Synergetic catalysis of palladium nanoparticles encaged within amine-functionalized UiO-66 in the hydrodeoxygenation of vanillin in water. *Green Chem.* **2016**, *18*, 2900–2908.
- (45) Hu, Z.; Peng, Y.; Kang, Z.; Qian, Y.; Zhao, D. A Modulated Hydrothermal (MHT) Approach for the Facile Synthesis of UiO-66-Type MOFs. *Inorg. Chem.* **2015**, *54*, 4862–8.
- (46) Zhang, X.; Dong, H.; Sun, X.-J.; Yang, D.-D.; Sheng, J.-L.; Tang, H.-L.; Meng, X.-B.; Zhang, F.-M. Step-by-Step Improving Photocatalytic Hydrogen Evolution Activity of NH₂-UiO-66 by Constructing Heterojunction and Encapsulating Carbon Nanodots. *ACS Sustainable Chem. Eng.* **2018**, *6*, 11563–11569.
- (47) Amer Hamzah, H.; Gee, W. J.; Raithby, P. R.; Teat, S. J.; Mahon, M. F.; Burrows, A. D. Post-Synthetic Mannich Chemistry on Metal–Organic Frameworks: System-Specific Reactivity and Functionality-Triggered Dissolution. *Chem. - Eur. J.* **2018**, *24*, 11094–11102.
- (48) Kim, M.; Cahill, J. F.; Prather, K. A.; Cohen, S. M. Postsynthetic modification at orthogonal reactive sites on mixed, bifunctional metal–organic frameworks. *Chem. Commun.* **2011**, *47*, 7629–7631.
- (49) Pachfule, P.; Yang, X.; Zhu, Q.-L.; Tsumori, N.; Uchida, T.; Xu, Q. From Ru nanoparticle-encapsulated metal–organic frameworks to highly catalytically active Cu/Ru nanoparticle-embedded porous carbon. *J. Mater. Chem. A* **2017**, *5*, 4835–4841.
- (50) Wang, J.-C.; Hu, Y.-H.; Chen, G.-J.; Dong, Y.-B. Cu(II)/Cu(0)@UiO-66-NH₂: base metal@MOFs as heterogeneous catalysts for olefin oxidation and reduction. *Chem. Commun.* **2016**, *52*, 13116–13119.
- (51) Shen, L.; Liang, S.; Wu, W.; Liang, R.; Wu, L. Multifunctional NH₂-mediated zirconium metal–organic framework as an efficient visible-light-driven photocatalyst for selective oxidation of alcohols and reduction of aqueous Cr(VI). *Dalton Trans.* **2013**, *42*, 13649–13657.
- (52) Kandiah, M.; Nilsen, M. H.; Usseglio, S.; Jakobsen, S.; Olsbye, U.; Tilset, M.; Larabi, C.; Quadrelli, E. A.; Bonino, F.; Lillerud, K. P. Synthesis and Stability of Tagged UiO-66 Zr-MOFs. *Chem. Mater.* **2010**, *22*, 6632–6640.
- (53) Mukoyoshi, M.; Kobayashi, H.; Kusada, K.; Hayashi, M.; Yamada, T.; Maesato, M.; Taylor, J. M.; Kubota, Y.; Kato, K.; Takata, M.; Yamamoto, T.; Matsumura, S.; Kitagawa, H. Hybrid materials of Ni NP@MOF prepared by a simple synthetic method. *Chem. Commun.* **2015**, *51*, 12463–12466.
- (54) Choi, S.; Watanabe, T.; Bae, T. H.; Sholl, D. S.; Jones, C. W. Modification of the Mg/DOBDC MOF with Amines to Enhance CO₂ Adsorption from Ultradilute Gases. *J. Phys. Chem. Lett.* **2012**, *3*, 1136–41.
- (55) Bae, Y.-S.; Farha, O. K.; Hupp, J. T.; Snurr, R. Q. Enhancement of CO₂/N₂ selectivity in a metal–organic framework by cavity modification. *J. Mater. Chem.* **2009**, *19*, 2131–2134.
- (56) Lin, A.; Ibrahim, A. A.; Arab, P.; El-Kaderi, H. M.; El-Shall, M. S. Palladium Nanoparticles Supported on Ce-Metal–Organic Framework for Efficient CO Oxidation and Low-Temperature CO₂ Capture. *ACS Appl. Mater. Interfaces* **2017**, *9*, 17961–17968.
- (57) Sharma, V.; De, D.; Saha, R.; Das, R.; Chattaraj, P. K.; Bharadwaj, P. K. A Cu(II)-MOF capable of fixing CO₂ from air and showing high capacity H₂ and CO₂ adsorption. *Chem. Commun.* **2017**, *53*, 13371–13374.
- (58) Pal, A.; Chand, S.; Das, M. C. A Water-Stable Twofold Interpenetrating Microporous MOF for Selective CO₂ Adsorption and Separation. *Inorg. Chem.* **2017**, *56*, 13991–13997.
- (59) McDonald, T. M.; D'Alessandro, D. M.; Krishna, R.; Long, J. R. Enhanced carbon dioxide capture upon incorporation of N,N'-dimethylethylenediamine in the metal–organic framework CuBTTri. *Chem. Sci.* **2011**, *2*, 2022–2028.
- (60) Liu, J.; Strachan, D. M.; Thallapally, P. K. Enhanced noble gas adsorption in Ag@MOF-74Ni. *Chem. Commun.* **2014**, *50*, 466–468.
- (61) Chen, S.; Lucier, B. E. G.; Luo, W.; Xie, X.; Feng, K.; Chan, H.; Terskikh, V. V.; Sun, X.; Sham, T.-K.; Workentin, M. S.; Huang, Y. Loading across the Periodic Table: Introducing 14 Different Metal Ions To Enhance Metal–Organic Framework Performance. *ACS Appl. Mater. Interfaces* **2018**, *10*, 30296–30305.
- (62) Montazerolghaem, M.; Aghamiri, S. F.; Tangestaninejad, S.; Talaie, M. R. A metal–organic framework MIL-101 doped with metal nanoparticles (Ni & Cu) and its effect on CO₂ adsorption properties. *RSC Adv.* **2016**, *6*, 632–640.
- (63) Kim, J.; Kim, S. N.; Jang, H. G.; Seo, G.; Ahn, W. S. CO₂ cycloaddition of styrene oxide over MOF catalysts. *Appl. Catal., A* **2013**, *453*, 175–180.
- (64) Kathalikkattil, A. C.; Tharun, J.; Roshan, R.; Soek, H.-G.; Park, D.-W. Efficient route for oxazolidinone synthesis using heterogeneous biopolymer catalysts from unactivated alkyl aziridine and CO₂ under mild conditions. *Appl. Catal., A* **2012**, *447–448*, 107–114.
- (65) Taherimehr, M.; Van de Voorde, B.; Wee, L. H.; Martens, J. A.; De Vos, D. E.; Pescarmona, P. P. Strategies for Enhancing the Catalytic Performance of Metal–Organic Frameworks in the Fixation of CO₂ into Cyclic Carbonates. *ChemSusChem* **2017**, *10*, 1283–1291.
- (66) Macias, E. E.; Ratnasamy, P.; Carreon, M. A. Catalytic activity of metal organic framework Cu₃(BTC)₂ in the cycloaddition of CO₂ to epichlorohydrin reaction. *Catal. Today* **2012**, *198*, 215–218.
- (67) Beattie, C.; North, M.; Villuendas, P.; Young, C. Influence of Temperature and Pressure on Cyclic Carbonate Synthesis Catalyzed by Bimetallic Aluminum Complexes and Application to Overall syn-Bis-hydroxylation of Alkenes. *J. Org. Chem.* **2013**, *78*, 419–426.
- (68) Xue, Z.; Jiang, J.; Ma, M.-G.; Li, M.-F.; Mu, T. Gadolinium-Based Metal–Organic Framework as an Efficient and Heterogeneous Catalyst To Activate Epoxides for Cycloaddition of CO₂ and Alcoholysis. *ACS Sustainable Chem. Eng.* **2017**, *5*, 2623–2631.
- (69) Nguyen, P. T. K.; Nguyen, H. T. D.; Nguyen, H. N.; Trickett, C. A.; Ton, Q. T.; Gutiérrez-Puebla, E.; Monge, M. A.; Cordova, K. E.; Gándara, F. New Metal–Organic Frameworks for Chemical Fixation of CO₂. *ACS Appl. Mater. Interfaces* **2018**, *10*, 733–744.
- (70) Kurisingal, J. F.; Babu, R.; Kim, S.-H.; Li, Y. X.; Chang, J.-S.; Cho, S. J.; Park, D.-W. Microwave-induced synthesis of a bimetallic charge-transfer metal organic framework: a promising host for the chemical fixation of CO₂. *Catal. Sci. Technol.* **2018**, *8*, 591–600.
- (71) Kurisingal, J. F.; Rachuri, Y.; Gu, Y.; Kim, G.-H.; Park, D.-W. Binary metal–organic frameworks: Catalysts for the efficient solvent-free CO₂ fixation reaction via cyclic carbonates synthesis. *Appl. Catal., A* **2019**, *571*, 1–11.
- (72) Patel, P.; Parmar, B.; Kureshy, R. I.; Khan, N.-u.; Suresh, E. Efficient Solvent-Free Carbon Dioxide Fixation Reactions with Epoxides Under Mild Conditions by Mixed-Ligand Zinc(II) Metal–Organic Frameworks. *ChemCatChem* **2018**, *10*, 2401–2408.
- (73) Patel, P.; Parmar, B.; Kureshy, R. I.; Khan, N.-u. H.; Suresh, E. Amine-functionalized Zn(II) MOF as an efficient multifunctional catalyst for CO₂ utilization and sulfoxidation reaction. *Dalton Trans.* **2018**, *47*, 8041–8051.